Title

Spatial and temporal variability of internal wave forcing on a coral reef

Journal

Journal of Physical Oceanography, 35(11)

ISSN

0022-3670

Authors

Leichter, James J
Deane, G B
Stokes, M D

Publication Date

2005-11-01

Peer reviewed

Spatial and Temporal Variability of Internal Wave Forcing on a Coral Reef

J. J. LEICHTER, G. B. DEANE, AND M. D. STOKES

Scripps Institution of Oceanography, University of California, San Diego, La Jolla, California

(Manuscript received 22 June 2004, in final form 4 May 2005)

ABSTRACT

The deployment of a dense spatial array of temperature sensors on a coral reef in the Florida Keys provided a unique view of the interaction of cool water incursions generated by internal waves with the three-dimensional reef bathymetry. Water temperature on the reef surface was sampled every 5 s at 100 points on a 100 m by 150 m grid with concomitant measurements of water column velocity and temperature from mid-May through mid-August 2003. Episodic incursions of cool, subsurface water were driven by periods of strong semidiurnal internal tide and higher-frequency internal wave activity. For every time step in the data record the mean profile of temperature as a function of depth is calculated with a 3-m vertical averaging length scale. Subtracting this mean profile from the raw record yields a within depth, horizontal temperature anomaly. Visualization through time of the anomaly mapped onto the measured reef bathymetry reveals episodic variability of thermal patchiness across the reef as well as persistent features associated with reef bathymetry. Variation in the nature of the cooling and resulting thermal heterogeneity among events and seasons suggests multiple modes of cool water incursion ranging from unbroken, tidal period internal waves to packets of higher-frequency, energetic, broken internal bores.

1. Introduction

Internal waves, broadly defined as gravity waves propagating within a density stratified water column, are common in a wide variety of coastal ocean habitats and lakes. Both in situ measurements and remote sensing have been used to observe ocean internal waves, and laboratory and numerical studies have furthered the development of theory to describe the underlying mechanics (e.g., Fu and Holt 1984; Apel et al. 1975; Haury et al. 1979; Kao et al. 1985; Helfrich and Melville 1986). In a typical coastal ocean case where density stratification is concentrated along a primary pycnocline, internal waves tend to travel from areas of generation near the shelf break toward shore along the density interface. These waves are well described by Korteweg–de Vries (KdV) theory and often evolve from a single wave at the shelf break into packets of higher-frequency waves moving toward shore (Helfrich 1992). As internal waves move into shallow water, they can shoal and eventually break. The shoaling and breaking dynamics are not described by KdV theory, but have been studied in a number of laboratory experiments with stratified water columns and uniform bottom slopes (e.g., Wallace and Wilkinson 1988; Helfrich and Melville 1986; Helfrich 1992).

Internal wave activity in the Straits of Florida has been the subject of a number of studies over the past 40 years or so, and some of the possible source mechanisms have been identified. Observations (e.g., Parr 1937; Schmitz and Richardson 1968; Soloviev et al. 2003) and theoretical modeling work (Niiler 1968; Stommel 1965) support the idea that a resonant interaction between the barotropic tide and an internal seiche set up across the straits drives internal wave activity. Because the frequency of the internal seiche depends on the depth of the thermocline, the strength of the coupling between the barotropic tide and the seiche is seasonally modulated with the periods of greatest activity occurring during the summer months. Spinoff eddies from the Gulf Stream can also modulate the depth of the thermocline and could also be a source of variability in internal wave activity (e.g., Soloviev et al. 2003; Lee and Mayer 1977; Lee et al. 1985).

Shoaling internal waves created offshore can run up a slope unbroken, or they can become unstable and break forming turbulent surges, variously described as "blobs", "boluses," or "bores" (Wallace and Wilkinson

Corresponding author address: J. J. Leichter, Scripps Institution of Oceanography, Mail Code 0227, 9500 Gilman Dr., La Jolla, CA 92093-0227.
E-mail: jleichter@ucsd.edu

1988; Helfrich 1992). On gradual slopes (<15°) most of the incident wave energy is dissipated in the shoaling and breaking process and little energy is reflected offshore (Wallace and Wilkinson 1988; Helfrich 1992). Wave instability and breaking has been estimated to account for approximately 5%–15% of the total energy dissipated (Wallace and Wilkinson 1988; Helfrich 1992). Under conditions of continuous stratification, internal wave energy is not constrained to travel along a distinct density interface, but propagates along paths or rays at angles to the horizontal. In areas where the slope angle is close to a critical angle for the internal wave rays, the internal wave energy intersecting the seafloor can be transferred into rapid near bottom currents parallel to the slope (Cacchione et al. 2002).

Internal wave breaking represents a significant source of turbulence and diapycnal mixing within the ocean (Gregg 1989; Taylor 1992), and the strong horizontal flows resulting from the interaction of internal waves with sloping topography can cause transport of sediments near the bed (Cacchione et al. 2002). In coastal regions vertical mixing associated with internal waves can result in significant input of deep-water nutrients into shallow environments (e.g., Sandstrom and Elliott 1984; Leichter et al. 2003). The strong internal wave activity on coral reefs in the Florida Keys is a significant source of dissolved nutrients (Leichter et al. 2003).

In contrast to the studies of internal waves shoaling over smooth bottoms, prior consideration of the interaction of shoaling internal waves with irregular bathymetry or rough surfaces has been more limited. These studies have considered internal waves with wavelengths on the order of hundreds of meters to tens of kilometers interacting with features of comparable scales such as midocean ridges and the continental shelf (Thorpe 2001a,b). In this study we describe temporal and spatial variability measured on scales of seconds to hours and tens to hundreds of meters occurring as internal bores run up the irregular surface of a coral reef in the Florida Keys. This reef slope is characterized by a prominent step at approximately 15-m depth and a series of 1–2-m-high coral spurs and sand channels extending downslope in the offshore direction from the step. The reef surface is further characterized by roughness on a scale of tens of centimeters to 1 m associated with individual coral heads, depressions, and small overhangs. The arrival of internal bores on the reef slope is marked by frequent surges of cool, subsurface water arriving at predominantly semidiurnal frequencies, particularly in summer when the water column seaward of the reef is strongly stratified (Leichter et al. 1998; Leichter et al. 2003). The arrival of the cool water fronts at this site is characterized by strong onshore transport and elevated concentrations of dissolved nutrients and plankton, which can be up to an order of magnitude higher than background levels (Leichter et al. 1998, 2003). Typical durations of the cool water events range from approximately 20 minutes to several hours, and prior observations suggest that the runup and dissipation of internal bores on the reef slope are affected by the reef bathymetry. For example, during the onshore flow, cool water appears to penetrate up the sand channels faster than the spurs and, after the main surge of water has receded offshore, isolated "pockets" of cool water can be observed in the sand channels, depressions, and under overhangs (authors' personal observations). Thus, the interaction of internal bores with the irregular surface of the reef may lead to elevated levels of mixing and the production of spatial patchiness of thermal variability and nutrient flux within the reef.

The scales of spatial patchiness and magnitude of thermal fluctuations driven by internal waves at Conch Reef may be of considerable biological importance to organisms such as corals and other sessile invertebrates that exist on scales of tens of centimeters to meters and are sensitive to small changes in temperature. While a larger array of current meters would be necessary to determine the exact fate of the cool water following incursion events, the duration of events on the order of tens of minutes to hours appears long enough and the events are sufficiently frequent for organisms such as suspension feeding corals and macroalgae to benefit from the enhanced availability of suspended particles and dissolved nutrients. Prior research at Conch Reef show enhanced growth rates of both benthic algae and suspension feeding corals associated with the enhanced fluxes of nutrients and suspended particles with internal waves (Leichter et al. 2003, 1998; Smith et al. 2004). On coral reefs, temperature variability, per se, is important because of physiological stresses in corals occurring at both high and low temperatures (Brown 1997; Knowlton and Jackson 2001) and also because temperature can be strongly inversely correlated with dissolved nutrient concentrations. Physical forcing associated with internal waves is known to occur both on other coral reefs (e.g., Wolanski and Pickard 1983; Wolanski and Hamner 1988; Wolanski and Delesalle 1995; Wolanski and Deleersnijder 1998) and in a wide variety of shallow water marine environments (e.g., Sandstrom and Elliott 1984; Holloway 1987; Pineda 1991; MacKinnon and Gregg 2003).

For this study we deployed a unique system [called the Benthic Oceanographic Array (BOA); Deane and Stokes (2002)] for sampling temperature variability on dense spatial scales. Deployed in a rectangular configu-

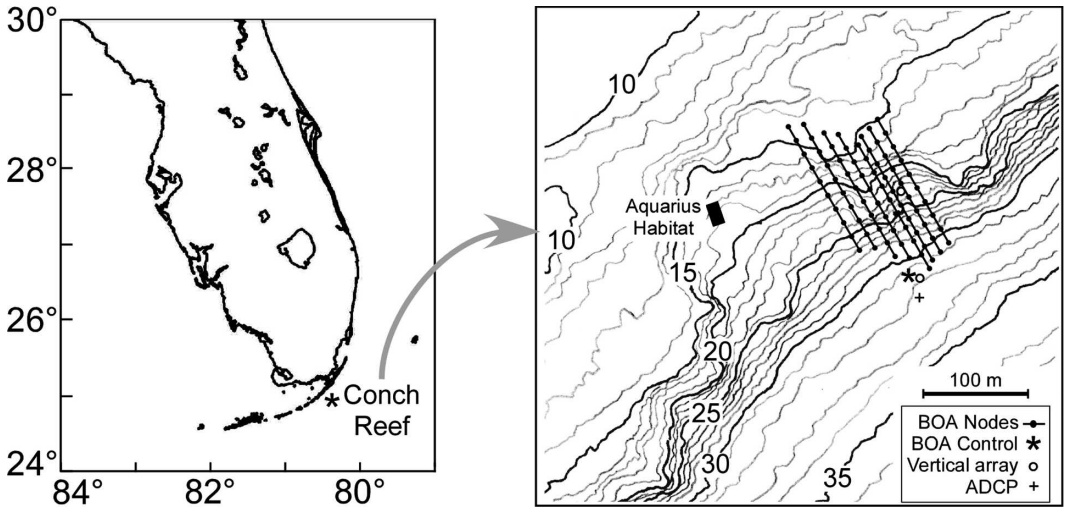

FIG. 1. Map of the study site at Conch Reef (24°57.0′N, 80°27.3′W) near the southern tip of Florida. Bathymetric contours (in 1-m intervals) and the approximate location of deployed instruments are shown on the right.

ration over a swath reef slope with additional vertical arrays and a profiling acoustic current meter, this system provided a uniquely detailed, time-evolving picture of internal tidal forcing over spatial scales of 10–100 m. This system allowed us to investigate the time-varying, three-dimensional thermal structure across the surface of the reef resulting from the interaction of internal wave surges with the reef topography at a scale of tens of meters.

2. Methods

a. Study site

This study was conducted on Conch Reef in the Florida Keys (24°57.0′N, 80°27.3′W), Fig. 1, a site of previous research on physical/biological coupling on the Florida Keys reef tract and the location of the Aquarius Habitat undersea laboratory operated by National Undersea Research Center (NURC) of the National Oceanic and Atmospheric Administration (NOAA). Conch Reef is similar to other reefs in the upper Florida Keys, consisting of a Holocene veneer of scleractinian corals, hydrozoans, sponges, coralline and filamentous and fleshy algae encrusting the Plio–Pleistocene carbonate platform. From the reef crest in 8–10-m depth the forereef slopes gradually (ca. 2%–5% slope) to a step at 15–18-m depth where the slope become steeper (ca. 8%–15% slope) down to the base of the reef at 30–32-m depth. A series of parallel, low (1–2-m height) coral spurs separated by sand channels runs down the forereef slope. A gradually sloping (ca. 1% slope) sand and carbonate plain extends seaward of the reef approximately 20–30 km to the deeper channel of the Straits of Florida. Alongshore currents on the reef are typically moderate to strong (0.1–0.5 m s^{-1}) toward the northeast, with tidal reversals to the southwest. Farther offshore (1–5 km) flow is strongly influenced by the Florida Current and is typically fast (0.5–2.0 m s^{-1}) toward the northeast. Surface tides are mixed semidiurnal with mean amplitude approximately 0.5–0.75 m.

Equipment in this study was deployed across depths from 15 to 32 m using SCUBA in May 2003, and the study site was surveyed and the instrumentation recovered in August 2003 during a 10-day Aquarius Habitat saturation diving mission. Water column profiles of conductivity and temperature seaward of the study sites were measured on 17 May and 8 August 2003 with a Seabird Electronics SBE-19 conductivity–temperature–depth (CTD) profiler. Individual CTD casts were made at 1.8-km intervals along a line extending seaward (150°) from Conch Reef to a station located 18 km offshore. Data for each cast were averaged into 1-m vertical bins. The Brunt–Väisälä buoyancy frequency was calculated as a function of the vertical density gradient (Pond and Pickard 1983) and smoothed with a 5-m running mean average.

b. Instrumentation

The primary technology for this study was a large temperature sensor array capable of synchronized, high precision, autonomous sampling for extended periods (Deane and Stokes 2002). The system consists of 100 temperature sensors arranged in 10 arrays of 10 elements spaced serially along cables at 15-m intervals.

This device, the Benthic Oceanographic Array, was deployed by divers on Conch Reef. The system allows sampling of all sensors at a 5-s interval with a resolution and accuracy of 0.007° and 0.04°C, respectively. Sensor nodes were anchored to the reef by fixing them to a 25-cm spike driven into the bottom. Array cables were also additionally anchored to the reef by tying them to dead coral outcroppings where convenient. The 10 cables were connected to a submersible junction box at the BOA control and power supply located at the base of the reef slope at 33-m depth (see Fig. 1). Data were recorded onto a 500-Mbyte flash memory card for the first 45 days at which time the control unit was recovered, downloaded, and redeployed for a second 40-day interval. The total operational period was 92 days from 17 May to 17 August 2003. Individual temperature recorders (Seabird Electronics SBE39, 0.002°C accuracy sampling at 10-s intervals) were deployed immediately adjacent to the BOA nodes at the deepest and shallowest corners of the array.

At the end of the study the location of the individual sensor nodes was surveyed by divers before the equipment was recovered. The survey was conducted on two length scales. A large-scale mapping was made of the BOA grid and reef topology using compass board, survey measuring tape, and digital depth gauge. This procedure located the node position to within <0.5 m spatially and approximately 0.3-m depth. These locations were surveyed relative to fixed markers on the seafloor (i.e., permanent moorings for the Aquarius habitat of known GPS position). A secondary survey was conducted near each node using a housed digital Nikon camera mounted on a frame encompassing an area of 0.25 m^2. Four images were taken covering a total area of 1.0 m^2 surrounding each node at each node to identify small-scale fluctuations in topography on the order of centimeters as well as to identify the substrate type and organisms living adjacent to the nodes.

An acoustic Doppler current profiler (ADCP) (RDI Workhorse 600 kHz) with pressure sensor was deployed near the BOA control and power supply at 32-m depth. This instrument sampled at 1.33 Hz and stored 1-min averages in 1-m vertical bins. Velocities were broken down into alongshore, cross-shore, and vertical components with the alongshore defined as parallel to the main reef axis, positive toward 45°, and the cross-shore defined as orthogonal to this axis, positive toward 315°. A vertical array of 12 individual temperature sensors (Onset Computers WaterTempPro, 0.2°C resolution, sampling at 0.5-Hz storing 5-min average values) spaced at 1-m intervals was deployed near the BOA control box at 32-m depth and a second vertical array of six sensors was deployed on the reef slope at 18-m depth (see Fig. 1).

c. Analysis

This section presents the principles and equations used in the analysis of temperature fluctuations across the array. We consider the temperature field across the reef at a given point in time to consist of two components: 1) the component that is purely dependent on depth and 2) any deviation at each node from simple depth dependence. The first component describes the strong vertical thermal stratification of the water column. At a given point in time this component is constant for all nodes at a given depth, and we refer to it as the temperature at constant depth. The second component corresponds to the deviation at each sampling node, and we refer to it as the horizontal temperature anomaly. If the temperature across the reef were stratified consistently with respect to depth (i.e., no horizontal gradients in temperature), then the value sampled at every node would correspond to the node's depth, and the horizontal temperature anomaly at every node would be zero. Conversely, any within-depth heterogeneity of temperature along isobaths results in nonzero values of the anomaly.

Because the thermal field is dominated by vertical gradients, isolating this component allows a detailed examination of the smaller, time-varying component contained in the anomaly and indicative of horizontal gradients. Spatial and temporal variation in the anomaly arises from a number of factors including the nature of the cool water incursions on the reef and their interaction with the reef bathymetry.

The two components of the temperature field across the reef can be defined mathematically as follows. As described above, there were 100 nodes positioned across the reef at locations (x_j, y_j, z_j), where $j = 1, 2, \ldots, 100$, is the node index and x, y, and z respectively are the across-shore, alongshore, and vertical distance from a fixed reference point on the reef. These true positions were surveyed with some error, such that

$$(\hat{x}_j, \hat{y}_j, \hat{z}_j) = (x_j + \tilde{x}_j, y_j + \tilde{y}_j, z_j + \tilde{z}_j), \tag{1}$$

where a caret indicates its measured value and a tilde indicates a normally distributed error. Applying this same notation to the temperature data, which were also measured with some error, the temperature recorded by node j at time t_k is

$$\hat{T}_j(t_k) = T_j(t_k) + \tilde{T}_j, \tag{2}$$

where $T_j(t_k)$ is the true water temperature.

We calculated the temperature at constant depth by taking the average of measured temperatures at all

nodes within a specified depth range. This is defined at node j by

$$\overline{T}_j(t_k; L) = \frac{1}{n} \sum_{i \in \Theta} T_i(t_k), \tag{3}$$

where L is a constant vertical length scale for the average, Θ is the set of nodes to average over with depths that satisfy $\hat{z}_j - L/2 \leq \hat{z}_i < \hat{z}_j + L/2$, and n is the number of nodes in the average. The horizontal anomaly at node j is the difference between the measured temperature and the temperature at constant depth, defined by

$$\alpha_j(t_k; L) = T_j(t_k) - \overline{T}_j(t_k; L). \tag{4}$$

Means and standard deviations of the anomaly can be calculated across a chosen time interval for a given node, or across the array (i.e., a spatial average) for a given sample time. The latter yields a single mean and standard deviation across the deployment region for each sampling interval.

Figure 2a shows an example of the depth profile of $\overline{T}_j$ (solid line) and the measured temperature at every node (points). This example corresponds to a period of relatively strong thermal stratification across the reef in late May. The anomaly at each node corresponds to the distance between plotted point and $\overline{T}_j$. As indicated in Eqs. (3) and (4), both $\overline{T}_j$ and the α_j are sensitive to the choice of L, the vertical length scale for averaging, chosen as 3 m.

The magnitude of L effectively determines the length scale of variability that is partitioned into the each of the two components of the overall temperature field. The effect of varying L on the calculation of the anomaly can be studied by processing profiles for different averaging lengths. A typical example during a cold water incursion is given in Fig. 2b, which shows variation in the standard deviation of the anomaly across the array with changing averaging length L. At the smallest averaging length scales most of the variability in the signal is captured in the computed depth dependent mean, and the anomaly is small. As the length scale for averaging is increased, the mean profile become correspondingly smoother and more residual variability is partitioned into the anomaly. A suitable choice for the averaging length is one that captures the inherent water column depth stratification in the mean profile and that partitions small-scales processes related to reef heterogeneity into the anomaly. A way to find the suitable scale is to look for a range of values of L over which the computed anomaly is relatively invariant, suggesting a separation of scales between processes associated with the main water column vertical structure and the processes associated with heterogeneity of interest on the reef. This range of values occurs between approximately 5 and 10 m in Fig. 2b. During very energetic events, this length can become as small as 3 m, and this is the scale we chosen for the analysis of the full dataset.

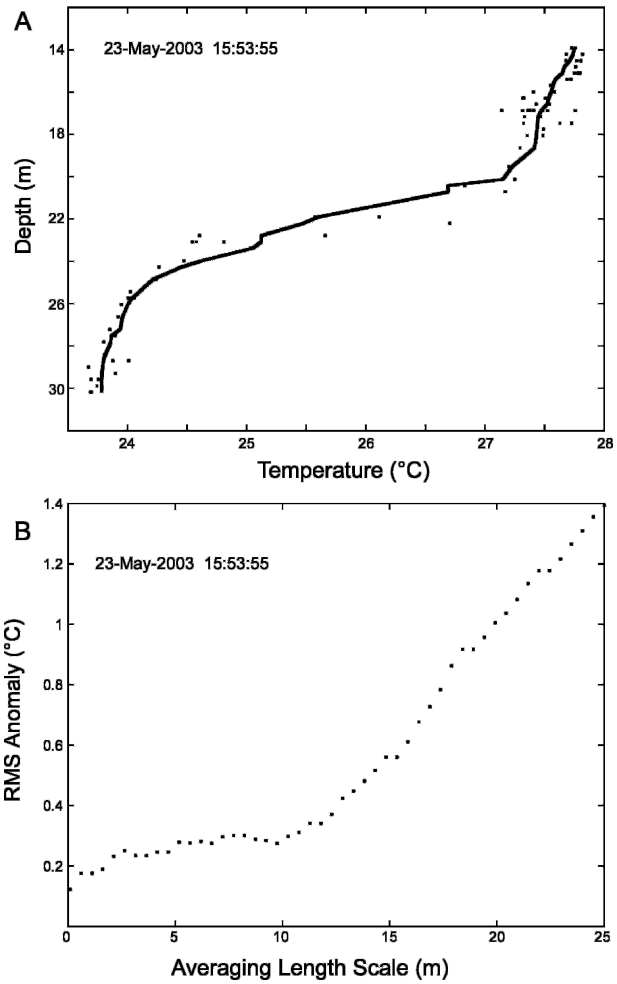

FIG. 2. (a) Example of the relationship between temperature and depth for a single time interval sampled across BOA. Dots represent the measured temperature at each node. Solid line represents the temperature averaged in 3-m-depth bins following Eq. (3). (b) Effect of varying the averaging length L [Eqs. (3), (4), and (5)] on the calculated total rms anomaly.

To improve the accuracy of the calculated anomaly, we performed an in situ calibration of the BOA nodes to estimate $\tilde{T}_j$. This was done by identifying five periods of unusually isothermal conditions throughout the deployment when the water temperature did not vary more than 10 millidegrees (m°C) at any node. The temperature anomaly during these periods was calculated as described above. Assuming that the anomaly was largely due to individual node calibration errors during

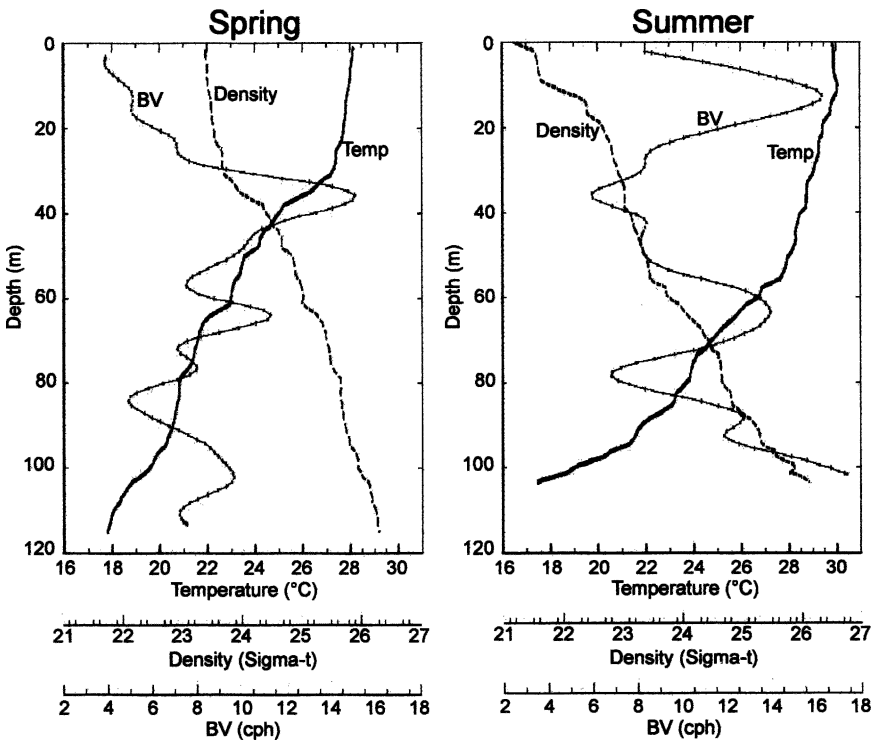

FIG. 3. Water column profiles of temperature (solid line), density (dashed line), and Brunt–Väisälä frequency (solid line with points in cycles per hour) for the station located 18 km seaward of the study site for spring (17 May) and summer (6 Aug) 2003.

these periods, this procedure yielded an estimate of the node constant offset values. In practice the anomaly will consist of thermal structure across the array in addition to the node errors, but this bias in the error estimates can be minimized by averaging across multiple periods. A histogram of the estimated calibration errors (not presented) showed a roughly normal distribution with a mean of 0.02 m°C and standard deviation of 57 m°C. This distribution is consistent with the distribution of errors expected from the laboratory thermal calibrations of the BOA nodes. The node calibration offset estimated in this manner was subtracted from the raw temperature time series at the beginning of the analysis.

To visualize the extensive dataset, values of the temperature and anomaly from all BOA nodes were interpolated as color contour surfaces on a 4-m grid and mapped onto the measured reef bathymetry. Successive frames can be viewed individually or animated as movies.

3. Results

a. Overall observations

The water column seaward of Conch Reef was strongly stratified with respect to temperature and density during the study period. The vertical structure of temperature (solid line), density (dashed line), and Brunt–Väisälä (BV) buoyancy frequency (solid line with circles) are shown in Fig. 3. These profiles were collected at the offshore station 18 km seaward of the reef at the beginning and near the end of the study on 17 May and 6 August, respectively. In both time periods the water column was characterized by a nearly isothermal surface layer overlying cooler water characterized by a continuous increases in density with depth. The BV frequency in both periods varied with depth, between approximately 4 and 16 cycles per hour associated with the relatively strong vertical density stratification. There was an overall 2°C warming of the surface layer from approximately 28°C in May to 30°C in August. This warming was accompanied by a deepening of the surface layer. Temperature at 100-m depth was approximately 19°C in both sampling periods.

The continuous record of temperature on the reef reflected the general warming trend of the surface layer evident in the hydrographic profiles, as well as extensive high-frequency variability superimposed on the trend. Figure 4 shows the complete temperature record at a shallow (15 m) and deep (30 m) node from 16 May to 17 August 2003. The short gap near the midpoint of

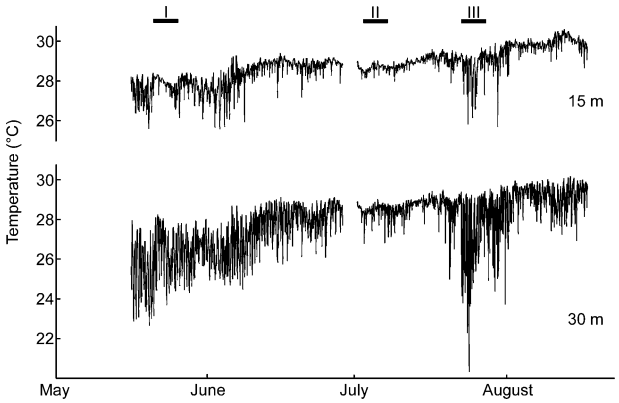

FIG. 4. Time series of temperature from individual nodes at 15- and 30-m depths on the reef. Horizontal bars refer to three 5-day portions of the overall record investigated in detail, I: 20–25 May; II: 2–7 Jul; and III: 22–27 Jul.

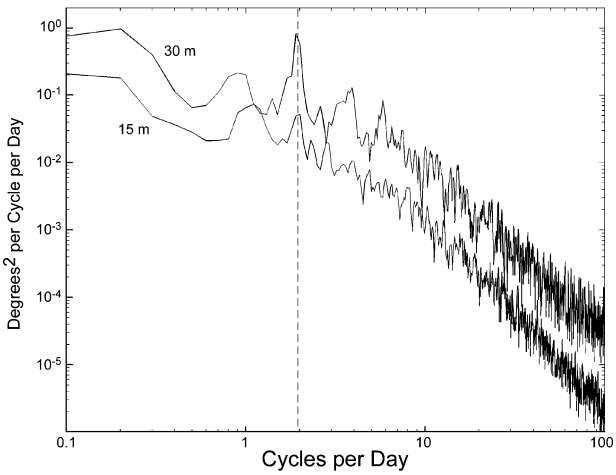

FIG. 5. Power spectral density estimate of the temperature time series from individual nodes at 15- and 30-m depths. Spectrum produced by Welch's method with nonoverlapping data sections 10 days long. Vertical line indicates M_2 frequency.

the record reflects approximately 3 days when the BOA control/power unit was retrieved, downloaded, and redeployed at the end of June. The high-frequency temperature variability consisted of numerous rapid fluctuations, some as large as 8°C at 30 m occurring on a time scale of minutes. The cooling events were associated with incursions of cool water onto the reef, often in the form of sharply defined thermal fronts. The subsequent warming was generally slower and characterized a more gradual flow of cool water down the reef slope. Consistent with prior observations (Leichter et al. 1996, 2003) the temperature variability was greatest near the base of the reef, with the amplitude of fluctuations varying episodically through time. The minimum temperatures, 20.3°C at 30 m and 25.7°C at 15 m, were recorded during a period of high variability and extensive cooling in late July. The maximum temperatures, 30.1°C at 30 m and 30.6°C at 15 m occurred in mid August. The solid bars at the top of Fig. 4 denote three 5-day periods of the overall record, which are focused upon in the detailed analysis below. These are periods of high variability in mid-May (I) and late July (III), as well as a period of relatively limited variability in early July (II).

Figure 5 shows power spectral density estimates calculated by Welch's average periodigram method for the temperature time series shown in Fig. 4. As noted above, the total variability was higher at 30 m than at 15 m. The relatively regular pattern of variability in the raw temperature record (especially evident in May and June) is reflected in the power spectrum as a distinct spectral peak corresponding closely to the semidiurnal (M_2) tidal frequency. This peak was present across depths, increasing in magnitude with depth. This observation is consistent with prior observations and shows strong semidiurnal temperature variability associated with internal waves of tidal frequency, which have greatest impact deep on the reef slope. The power spectra also show considerable energy at frequencies higher than M_2. Figure 5 shows the variability in wave frequency content across the entire data record at two depths. Figure 6 shows the time-varying frequency content from a node at the bottom of the reef (node 51) plotted as a color contour versus time and log frequency. The same estimation scheme was used as for Fig. 5 except that 5-day time periods were used. Because the energy in the spectrum varies by several orders of magnitude, the plot has been divided into two frequency bands with two different color scales. There are two points worth noting. The first is that the M_2 tidal component shows up relatively strongly during late August and June but is less conspicuous during July and August. Although there is high-frequency energy evident throughout the entire data record, the energetic bursts of activity during August contain noticeably more high-frequency energy (greater than 10–20 cycles per day) than other periods.

b. Temperature anomaly through time

As described above, the thermal field is partitioned into two components, one describing the mean depth dependent stratification and the second describing the within-depth horizontal anomaly at every sampling node. Figure 7 shows the time series of the standard deviation of the temperature anomaly calculated across the entire array in every sampling interval. Variation of the anomaly through time is associated with variation in

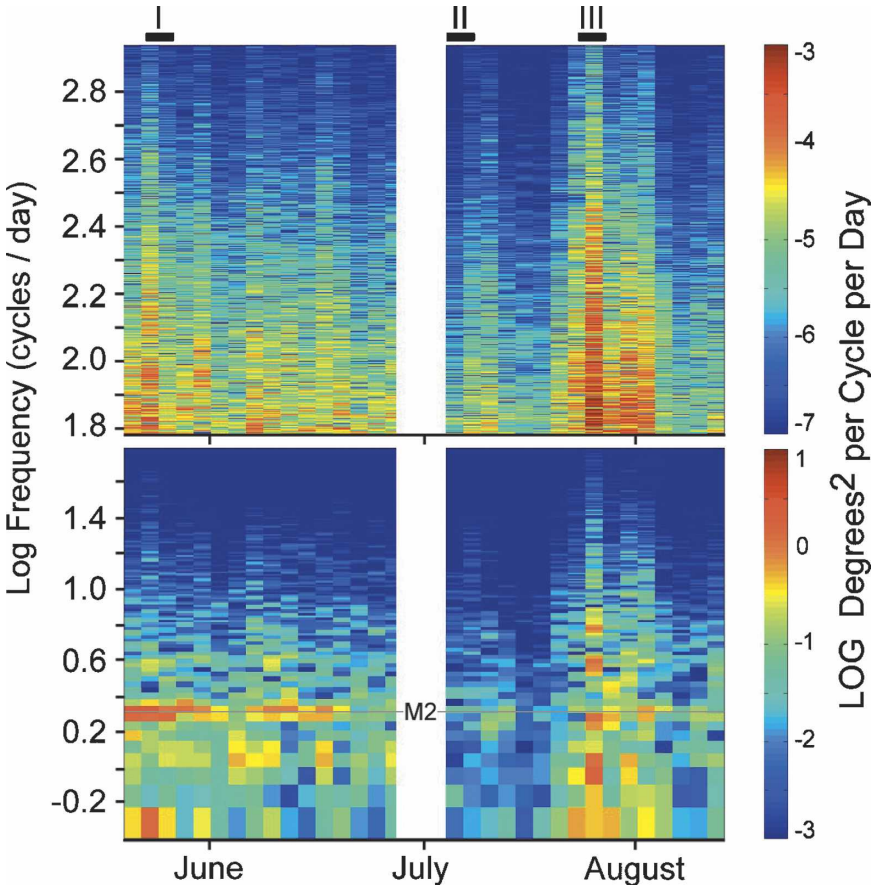

FIG. 6. Color contour map of the temperature power spectral density measured at the base of the reef and plotted vs frequency (in log cycles per day) and time. Each spectral estimate represents five days of data and has been broken into two frequency ranges to accommodate a high dynamic range. The M_2 line is annotated. Horizontal lines refer to three 5-day portions of the overall record discussed in detail, I: 20–25 May; II: 2–7 Jul; and III: 22–27 Jul.

the raw temperature record (see Fig. 4), with peak values of the anomaly corresponding with periods of high temperature variability associated with cool water incursions. The anomaly standard deviation was greatest (0.85°C) during the highly variable period in late July (period III) and was also large in mid-May (period I) and early June. The anomaly was consistently small during early July (period II) when temperature variability on the reef was minimal. Figure 8 shows the relationship between the reef temperature anomaly (dashed line) and barotropic tide (solid line) measured by pressure at the ADCP at the base of the reef in periods I and III. Both signals have been smoothed with a 2-h low-pass Chebechev filter. During period I the temperature anomaly was tightly correlated and nearly in phase with the semidiurnal tidal pressure signal and the associated strong, semidiurnal cooling on the reef (see Fig. 4). During period III the temperature anomaly across the reef varied significantly faster than the tidal pressure signal. The temperature signal in this time period was characterized by numerous bouts of rapid cooling occurring as series of rapid pulses of cool water onto the reef (see Fig. 4 and Fig. 9b).

Nonzero values of the anomaly imply node-specific deviations from the mean profile of temperature with depth. These deviations can arise from two sources: 1)

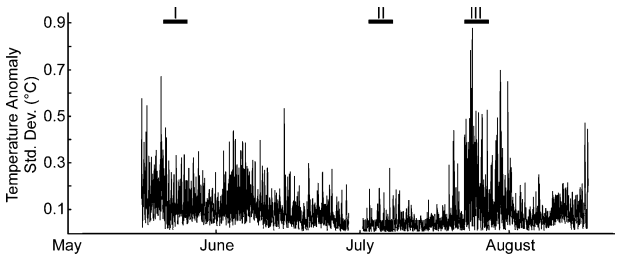

FIG. 7. Standard deviation of the instantaneous temperature anomaly. Horizontal bars refer to same time periods as in Fig. 4.

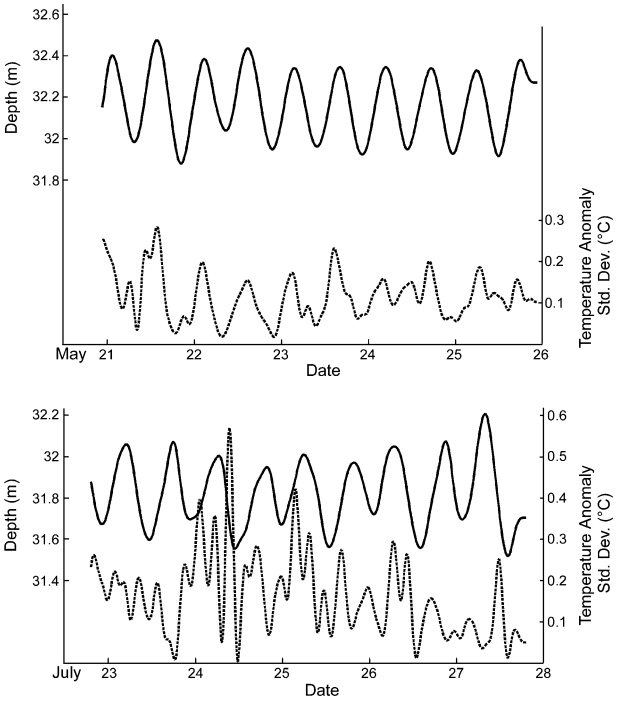

FIG. 8. Depth (solid line) measured by the ADCP pressure sensor at the base of the reef and standard deviation of the temperature anomaly across the reef (dashed line) for periods (top) I and (bottom) III.

along-isobath thermal structure and/or 2) measurement error. Measurement errors could arise from node calibration error, causing a specific node to read consistently above or below the true temperature, and/or from node survey depth. As described above, node temperature calibration error was minimized by subtracting the small, node-specific temperature offset calculated from several short time periods of isothermal conditions across the reef. The error in node depths associated with the resolution of the digital depth gauge was approximately 0.30 m, and additional possible variations associated with small changes in tidal height during the survey (which were minimized by conducting surveys at approximately the same tidal phase a few successive days) bring the estimated total depth error to 0.50 m. While thermal structure at vertical scales less than 0.50 m may have existed at times during the deployment, these small-scale thermal fluctuations should average to zero across the reef and are unlikely to have contributed significantly to the large fluctuations in the magnitude of the anomaly through time.

The physically interesting sources of the anomaly include a range of potential factors that can produce instantaneous horizontal thermal structure and heterogeneity on the reef. These include 1) channeling of cool water into reef features such as sand grooves during the runup and subsequent recession of internal bores, 2) retention and pooling of warm or cool water masses in features such as depressions on the reef, 3) impingement of internal bores onto the reef slope at an angle relative to the alongshore direction, 4) turbulence and mixing imbedded in the incident cool water incursions and/or associated with the interaction of cool water incursions with reef bathymetric features, and 5) interactions between the incident cool water incursions, the reef bathymetry, and the strong alongshore flow above the reef. Factors specifically tied to reef bathymetry can be expected to lead to persistent areas of positive or negative thermal anomalies that can be mapped onto the reef surface.

c. *Spatial patterns and structure of individual events*

The nature of the cool water incursions and their relation to the temperature anomaly can be examined in detail by focusing on specific events. Figure 9 shows the vertical structure of temperature and currents above the reef for 24-h periods on 18 May (Fig. 9a) and 24 July (Fig. 9b) 2003. The across-shore temperature was taken from the horizontal BOA array coincident with the vertical temperature strings. On 18 May the arrival of cool water on the reef was associated with onshore flow speeds of approximately 5–15 cm s^{-1} as the reef was gradually blanketed by cool water. The time series of the vertical thermal structure above the deep edge of the reef (semitransparent panes in Fig. 9) shows a lag in the temperature change at sensors successively up the vertical array. This suggests the movement onto and subsequent recession off of the reef of a thermally stratified layer. By contrast, the cooling events on 24 July were associated with the arrival of sharp fronts of cool water, arriving as a series of energetic pulses with cross shore velocities between 25 and 30 cm s^{-1} and oscillating upward and downward vertical velocities. During these events the vertical arrays show all sensors within the bottom 2–10 m of the water column detecting the temperature change at nearly the same time. These observations suggest that the 24 July events were characterized by rapid movement onto the reef of cool water bores that were internally vertically mixed.

Figure 10 shows the temperature field mapped onto the reef bathymetry for the cooling events on 23 May (Fig. 10a) and 24 July (Fig. 10b). On 23 May, the temperature contours tended to follow the contours of reef bathymetry during both the incursion and recession of cool water. In contrast, the rapidly moving cool water incursions on 24 July showed significant horizontal structure along isobaths.

Figure 11 shows instantaneous values of the horizontal temperature anomaly mapped onto the reef bathym-

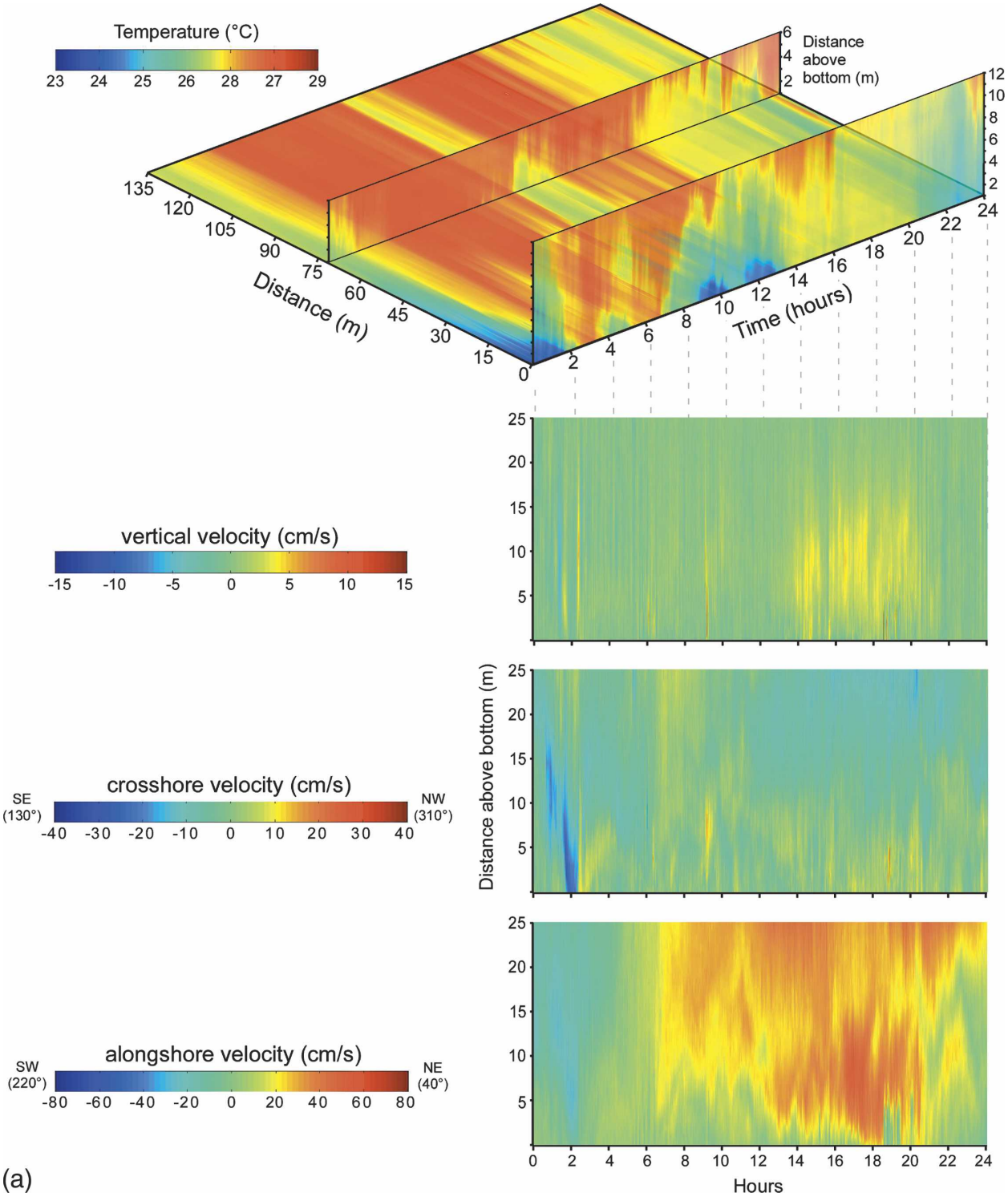

FIG. 9. (top) Bottom and water column temperature and (bottom) cross-shore, vertical, and alongshore components of currents for 24-h periods in (a) spring (18 May) and (b) summer (24 Jul). The vertical panes are rendered semitransparent, showing temperature at the vertical arrays next to the BOA control/power unit and halfway up the reef. Axes indicate time and distance in meters up the reef slope from the BOA control unit.

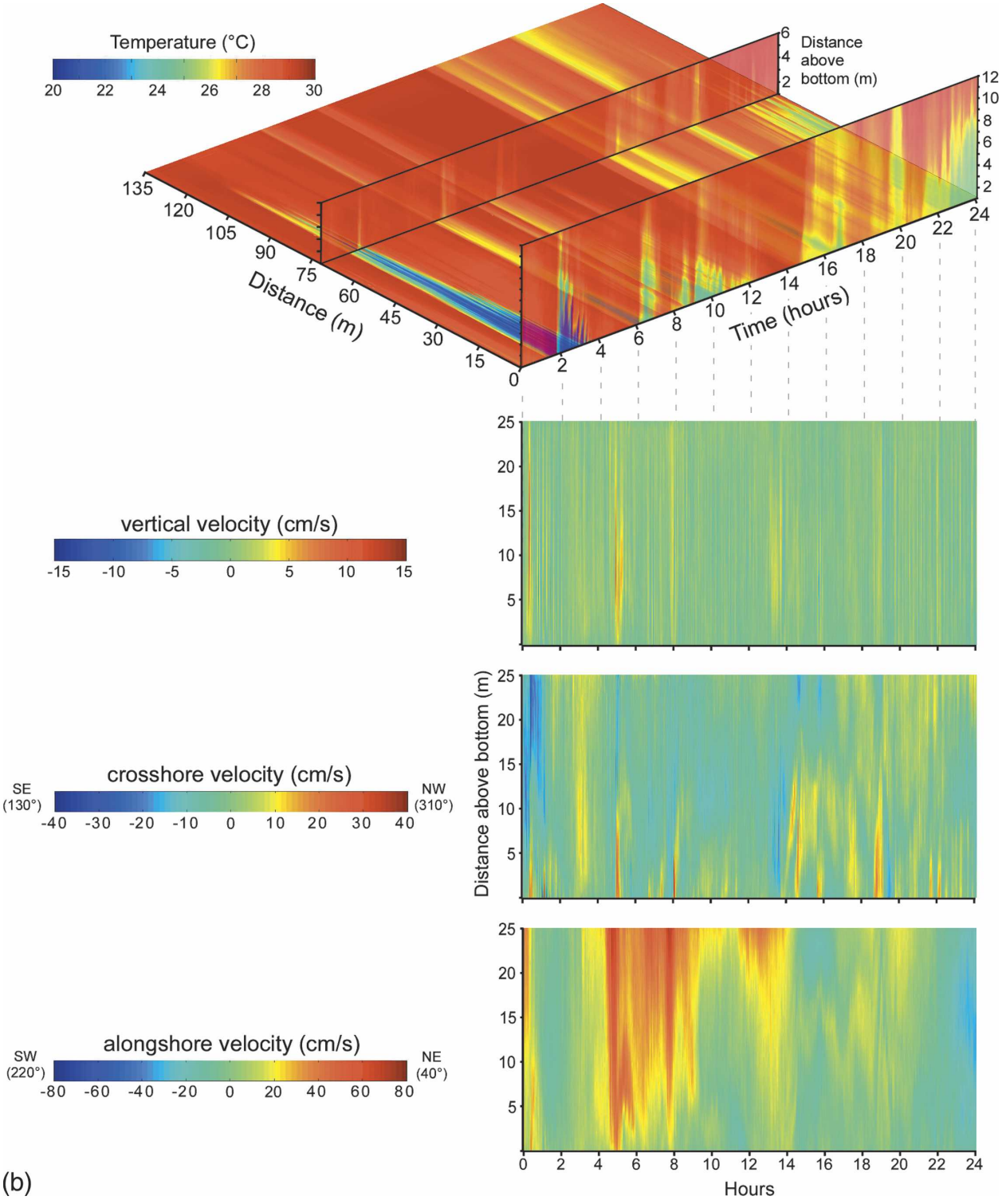

FIG. 9. (*Continued*)

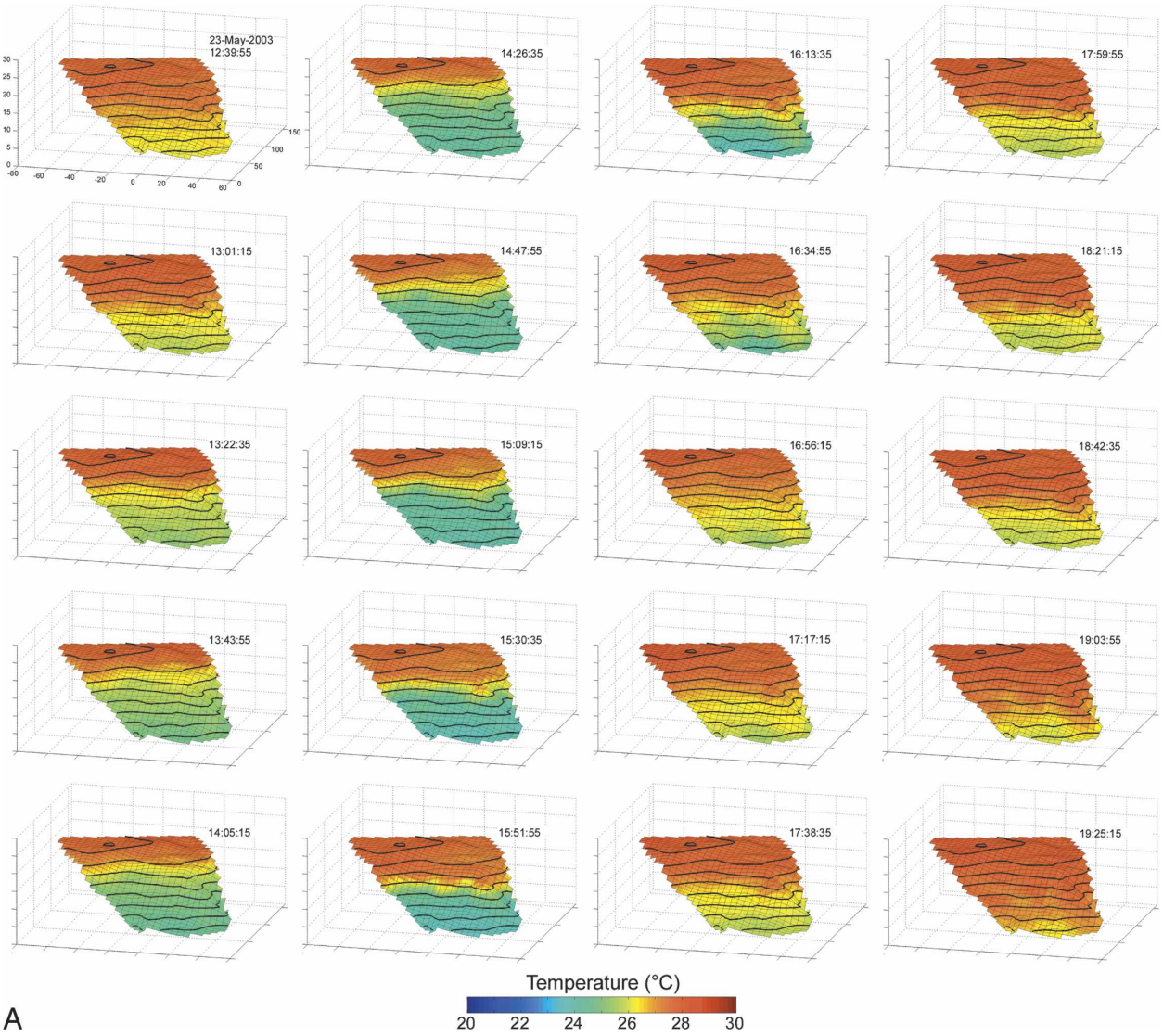

FIG. 10. Sequential images (reading down columns) of water temperature interpolated onto the reef bathymetry for two time periods: (a) 20 frames at approximately 21-min intervals spanning approximately 7 h on 23 May 2003 and (b) 20 frames at approximately 5-min intervals spanning approximately 2 h on 24 Jul 2003. Dark lines show bathymetric contours at 2-m intervals. Axis scales are in meters relative to a fixed point at the southeast corner of the array.

etry for the 23 May (Fig. 11a) and 24 July (Fig. 11b). The overall state of the cold water incursion driving the anomaly can be seen in Fig. 10. As expected from the close correspondence between temperature and bathymetry contours during this cold water incursion, the temperature anomaly was relatively small across the array. By contrast, on 24 July the advancing cool water fronts were associated with high spatial heterogeneity across the reef. Areas of both anomalously cool and warm water are evident across the reef with distinct warm anomalies associated with the seaward edges of the reef spur and cool anomalies associated with the sand grooves.

Figure 12 shows 5-day averages of the temperature anomaly from each node interpolated onto the reef bathymetry for periods I, II, and III. During period II, when significant thermal variation was absent, the thermal anomaly is correspondingly low. In both periods I and III a distinct area of positive anomaly is evident near the lower right of the figure. This corresponds to a major spur on the reef. In the energetic period III a second area of overall positive anomaly is evident corresponding to the smaller spur at the lower left of the figure. The panels in Fig. 12, corresponding to periods I and III, show very similar patterns of temperature anomaly. To ensure that the patterns are, in fact, asso-

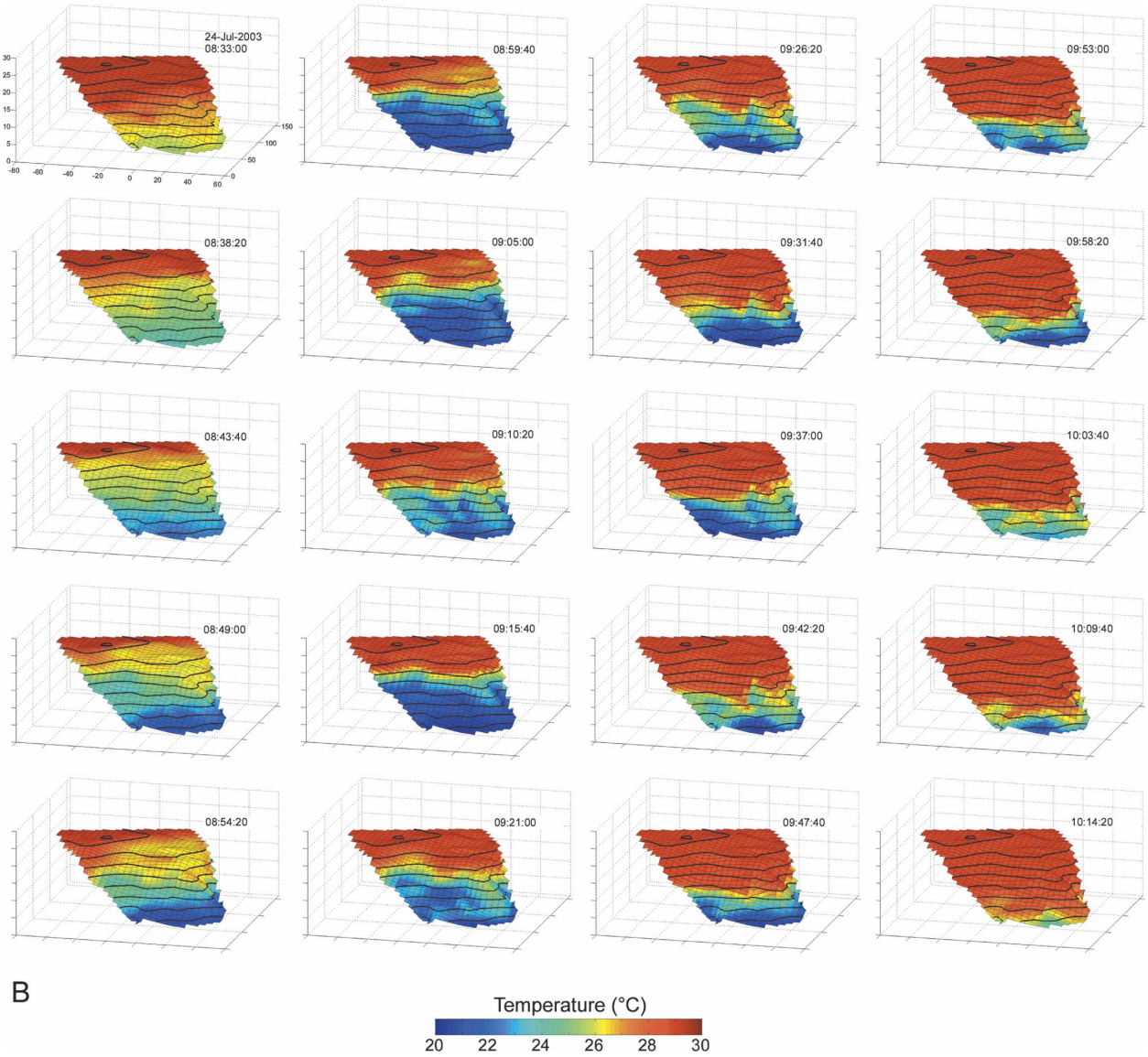

FIG. 10. (*Continued*)

ciated with wave–bathymetry interactions and not an artifact of node positional error, the anomaly analysis was rerun for period III after introducing a random offset into the node depths (0.5-m standard deviation, 0 mean Gaussian random offset). The analysis showed that the anomaly calculations are insensitive to depths errors of this magnitude, and, in particular, the two distinctive anomalies associated with the spurs at the leading edge of the reef were unchanged.

4. Conclusions

This study represents, to our knowledge, the first in situ, high-frequency, and three-dimensional view of the runup of internal waves on a complex surface such as a coral reef. Sequences of the overall temperature field and the calculated horizontal anomaly mapped onto the reef bathymetry clearly resolve patterns associated with cool water incursions at scales of meters to tens of meters in both the along- and cross-shore directions. The, within depth, horizontal temperature anomaly and the standard deviation of the anomaly for the entire array through time are useful metrics of spatial heterogeneity independent of the main variability associated with the strong stratification of temperature with depth. The horizontal temperature anomaly may be a useful proxy for processes such as turbulence and mixing that can be expected to contribute strongly to spatial het-

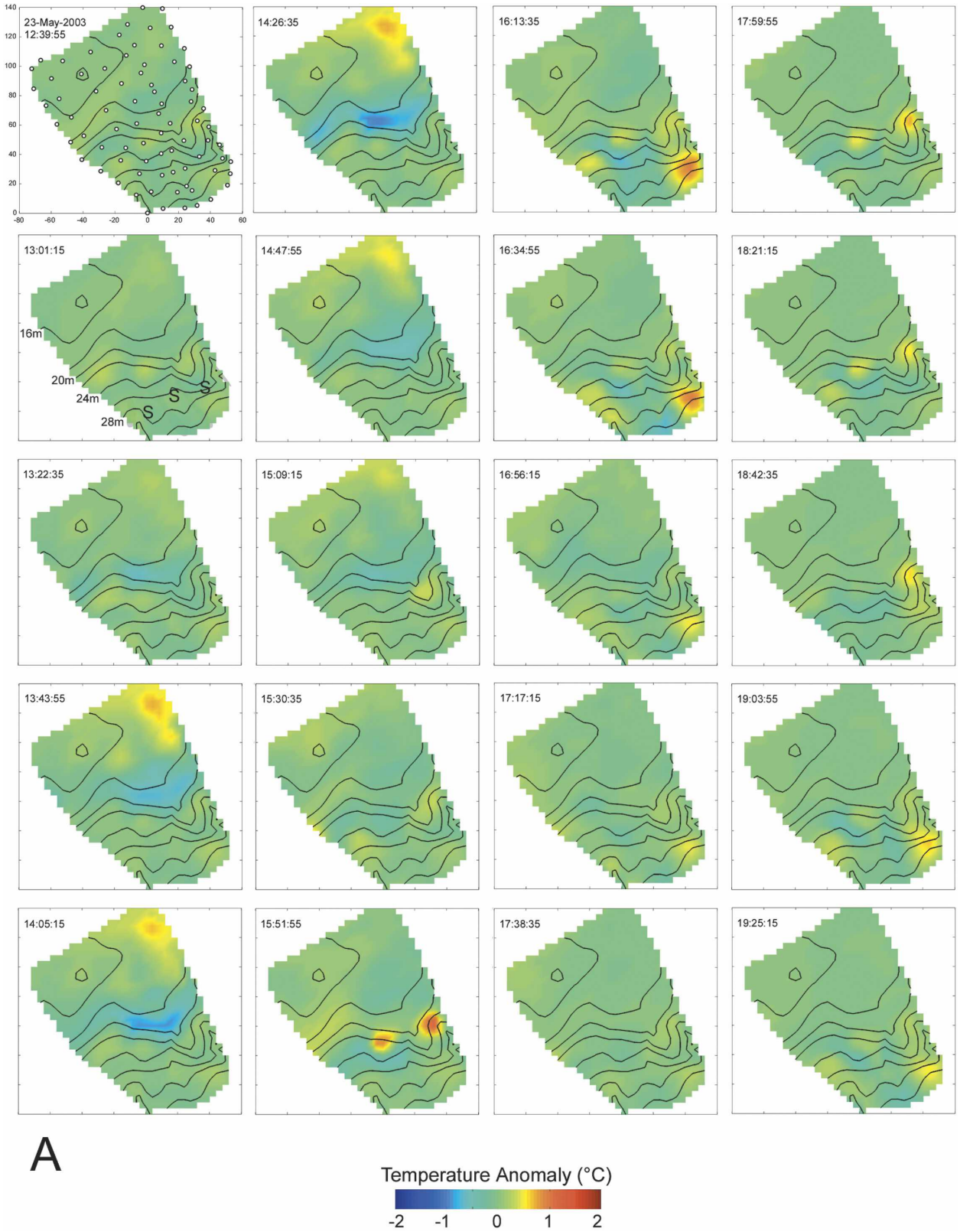

FIG. 11. Sequential images (reading down columns) of the instantaneous horizontal temperature anomaly [Eq. (4)] interpolated onto the reef bathymetry. Time periods and number and interval of frames same as in Fig. 9. Dark lines show bathymetric contours at 2-m intervals.

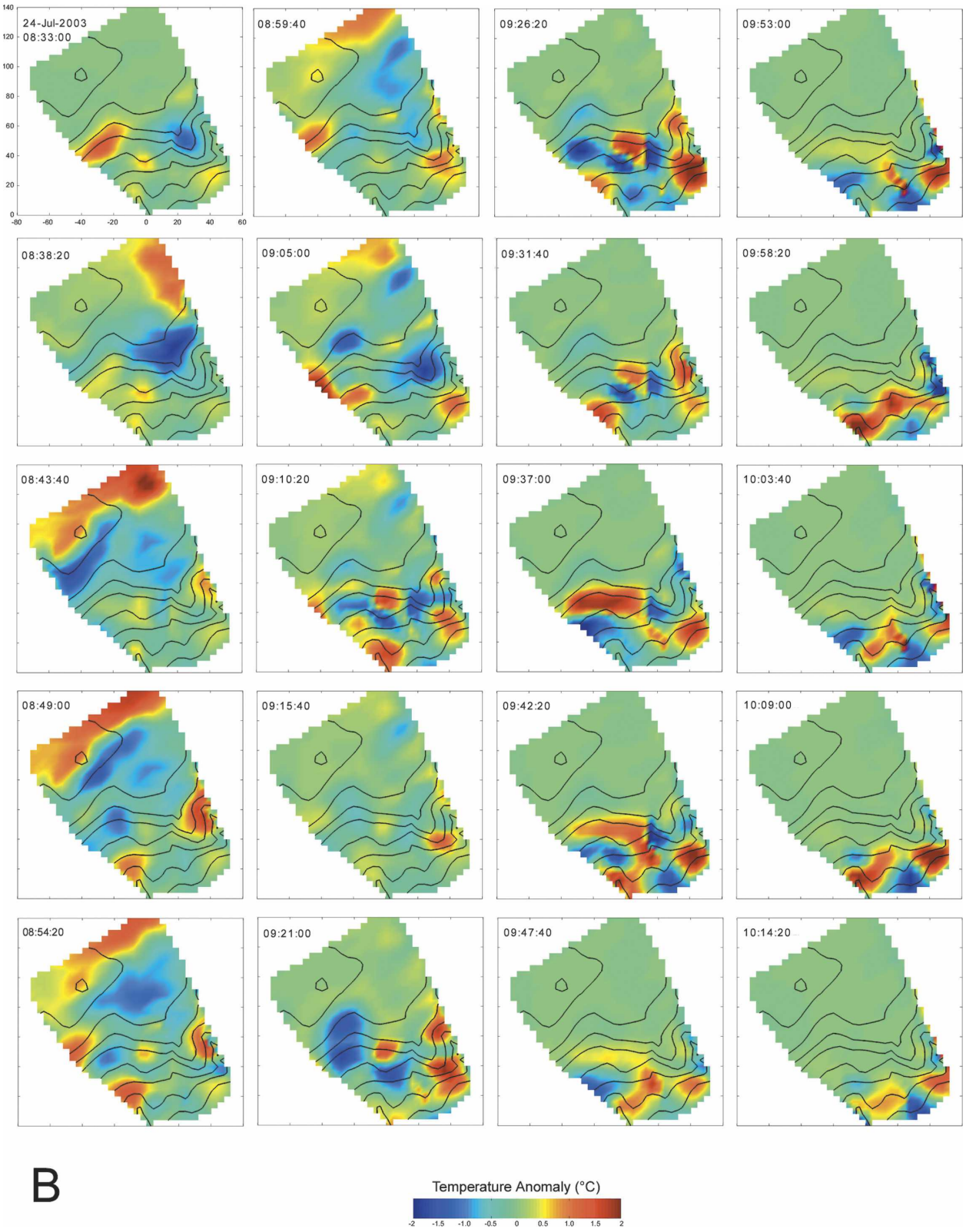

FIG. 11. (*Continued*)

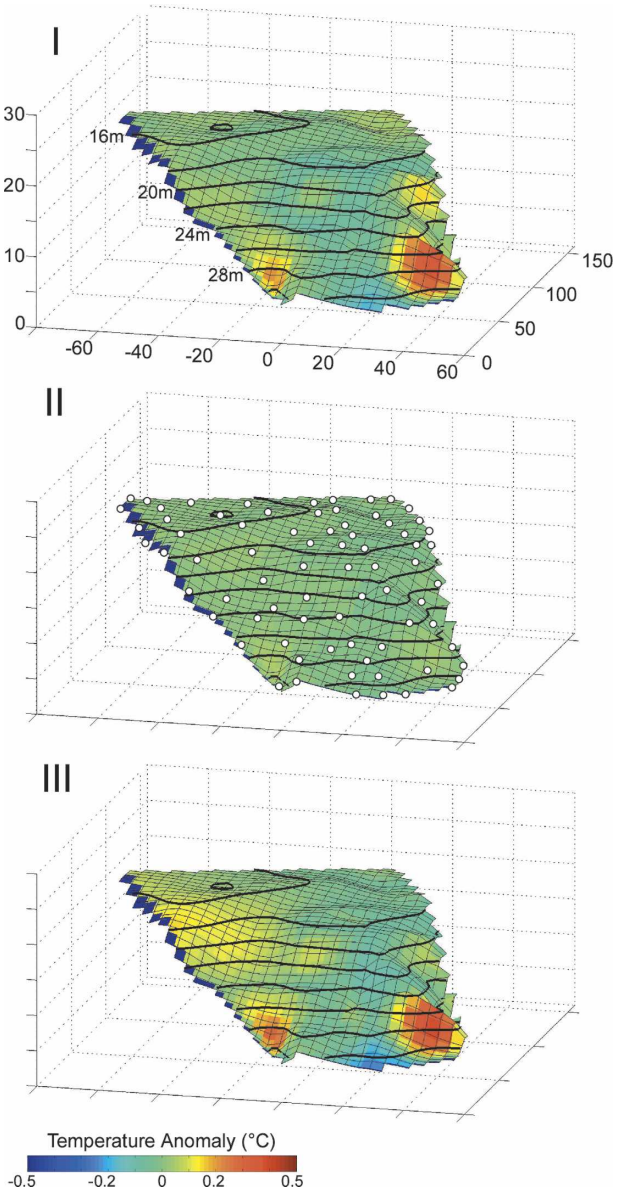

FIG. 12. Mean horizontal temperature anomaly for periods I, II, and III.

erogeneity. Fluctuations in the anomaly are closely linked to the frequency and magnitude of cool water incursions. The data also suggest differences in the mode of forcing between spring and summer.

In the spring (May/June) the temperature variability was dominated by a series of regularly spaced, cool water incursions correlated with the semidiurnal tidal frequency. We interpret this as the regular ebb and flood of internal waves of tidal period (an "internal tide"). At the advancing front, density contours conform well to the gross bathymetry of the reef as a vertical thermal gradient moves onto the reef. This suggests that the underlying internal wave is unbroken. In summer (July/August), the cool water incursions appeared more energetic and often arrived as packets or sets of onshore pulses accompanied by marked spatial heterogeneity across the reef. We interpret these events as the runup onto the reef of higher-frequency internal waves that have broken into rapidly advancing, turbulent internal bores ("internal surf"). The extent of turbulent energy dissipation, mixing, and fate of material transported onshore with the advancing cool water fronts are all likely to vary with the type of forcing event. These "types" of events likely represent points along a spectrum of variability associated with a broad range of possible frequencies of internal waves. Internal waves of varying frequency can also co-occur and overlap, for example in events where the onshore movement of the leading edge of the internal tide is also accompanied by a set of higher-frequency internal waves.

The seasonality of high-frequency forcing on Conch Reef is likely related to variation both in the structure of the offshore thermocline and of the mechanisms driving internal waves. In addition to predictable changes in water column density structure associated with seasonal warming in summer and increased mixing in winter, the structure of the offshore pycnocline can be modulated on time scales of days to weeks by eddies and meanders of the Florida Current (Mooers and Brooks 1977; Lee and Mayer 1977; Lee et al. 1985). The specific mechanisms generating the internal waves that impact Conch Reef and the locations of generation, shoaling, and possible breaking have not been resolved. Generating mechanisms are likely to include tidally forced currents interacting with the density stratified water column at or near the shelf break (Baines 1986). Resonant effects within the Florida Straits may also be important (Niiler 1968; Soloviev et al. 2003).

Observations of spatial patchiness over scales of meters to hundreds of meters are hampered by the prohibitive cost of deploying large numbers of recording instruments. Low-cost recording systems are available, but they generally suffer from problems of low thermal resolution, slow response times, and lack of sampling synchronization over extended deployment periods. The net result is that little is known about the spatial variability and the processes that cause it at scales most relevant to individual, benthic organisms. Deploying an array the size of BOA is a feasible, but work-intensive endeavor. It would be preferable to obtain the kinds of results presented here through measurement of the incident water masses using a few offshore vertical arrays combined with models for the interaction of internal

waves with three-dimensional topographic features on the seafloor. Detailed knowledge of the bathymetry at Conch Reef and an understanding of the underlying mechanisms of internal wave forcing could provide a base for developing such models, which could be tested against the present BOA dataset. Such an approach could increase our understanding of bathymetrically induced mixing in this system and of the interaction of internal waves with the strong alongshore velocity field above the reef.

Acknowledgments. We thank the following individuals who made this research possible: S. Miller and the support personnel at the National Undersea Research Center in Key Largo, Florida, as well as divers M. Murray, A. Coyac, C. Zilberberg, S. Curless, M. Simoncini, and boat captains M. Birns and K. Boykin. J. Uylon and C. Humphries assisted with the fabrication and calibration of the BOA. We thank D. Farmer for valuable discussions. Comments from two anonymous reviewers helped to sharpen the analysis and greatly improved the manuscript. Funding for the field research was provided by NSF (OCE 0239449) and NOAA UNCW/NURC. Fabrication of BOA was made possible by an award from the Ocean-Instrumentation division of the National Science Foundation (0220400).

REFERENCES

Apel, J. R., J. R. Proni, H. M. Byrne, and R. L. Sellers, 1975: Near simultaneous observations of intermittent internal waves on continental shelf from ship and spacecraft. *Geophys. Res. Lett.,* **2,** 128–131.

Baines, P. G., 1986: Internal tides, internal waves, and near-inertial motions. *Baroclinic Processes on Continental Shelves*, N. K. Moores, Ed., Amer. Geophys. Union, 19–31.

Brown, B. E., 1997: Coral bleaching: Causes and consequences. *Coral Reefs,* **16,** S129–S138.

Cacchione, D. A., L. F. Pratson, and A. S. Ogston, 2002: The shaping of continental slopes by internal tides. *Science,* **296,** 724–727.

Deane, G. B., and M. D. Stokes, 2002: A robust single-cable sensor array for oceanographic use. *IEEE Oceanic Eng.,* **27,** 760–767.

Fu, L. L., and B. Holt, 1984: Internal waves in the Gulf of California—Observations from a spaceborne radar. *J. Geophys. Res.,* **89C,** 2053–2060.

Gregg, M. C., 1989: Scaling turbulent dissipation in the thermocline. *J. Geophys. Res.,* **94C,** 9686–9698.

Haury, L. R., M. G. Briscoe, and M. H. Orr, 1979: Tidally generated internal wave packets in Massachusetts Bay. *Nature,* **278,** 312–317.

Helfrich, K. R., 1992: Internal solitary wave breaking and run-up on a uniform slope. *J. Fluid Mech.,* **243,** 133–154.

——, and W. K. Melville, 1986: On long nonlinear internal waves over slope-shelf topography. *J. Fluid Mech.,* **167,** 285–308.

Holloway, P. E., 1987: Internal hydraulic jumps and solitons at a shelf break region on the Australian North West shelf. *J. Geophys. Res.,* **92,** 5405–5416.

Kao, T. W., F. S. Pan, and D. Renouard, 1985: Internal solitons on the pycnoclyne: Generation, propagation, and shoaling and breaking over a slope. *J. Fluid Mech.,* **159,** 19–53.

Knowlton, N., and J. B. C. Jackson, 2001: The ecology of coral reefs. *Marine Community Ecology*, M. D. Bertness, S. D. Gaines, and M. E. Hay, Eds., Sinauer Associates, Inc., 395–422.

Lee, T. N., and D. A. Mayer, 1977: Low-frequency current variability and spin-off eddies along shelf off southeast Florida. *J. Mar. Res.,* **35,** 193–220.

——, F. A. Schott, and R. Zantopp, 1985: Florida current low-frequency variability as observed with moored current meters during April 1982 to June 1983. *Science,* **227,** 298–302.

Leichter, J. J., S. R. Wing, S. L. Miller, and M. W. Denny, 1996: Pulsed delivery of subthermocline water to Conch Reef (Florida Keys) by internal tidal bores. *Limnol. Oceanogr.,* **41,** 1490–1501.

——, G. Shellenbarger, S. J. Genovese, and S. R. Wing, 1998: Breaking internal waves on a Florida (USA) coral reef: A plankton pump at work? *Mar. Ecol. Prog. Series,* **166,** 83–97.

——, H. L. Stewart, and S. L. Miller, 2003: Episodic nutrient transport to Florida coral reefs. *Limnol. Oceanogr.,* **48,** 1394–1407.

MacKinnon, J. A., and M. C. Gregg, 2003: Mixing on the late-summer New England shelf—Solibores, shear, and stratification. *J. Phys. Oceanogr.,* **33,** 1476–1492.

Mooers, C. N. K., and D. A. Brooks, 1977: Fluctuations in the Florida Current, summer 1970. *Deep-Sea Res.,* **24,** 399–425.

Niiler, P. N., 1968: On the internal tidal motion in the Florida Straits. *Deep-Sea Res.,* **15,** 113–123.

Parr, A. E., 1937: Report on hydrographic observations in a series of anchor stations across the Straits of Florida. *Bull. Bingham Oceanogr. Coll.,* **6,** 1–63.

Pineda, J., 1991: Predictable upwelling and the shoreward transport of planktonic larvae by internal tidal bores. *Science,* **253,** 548–551.

Pond, S., and G. L. Pickard, 1983: *Introductory Dynamical Oceanography.* Pergamon Press, 329 pp.

Sandstrom, H., and J. A. Elliott, 1984: Internal tidae and solitons on the Scotian shelf: A nutrient pump at work. *J. Geophys. Res.,* **89,** 6415–6426.

Schmitz, W. J., and W. S. Richardson, 1968: On the transport of the Florida current. *Deep-Sea Res.,* **15,** 679–693.

Smith, J. E., C. M. Smith, P. S. Vroom, K. L. Beach, and S. L. Miller, 2004: Nutrient and growth dynamics of Halimeda tuna on Conch Reef, Florida Keys: Possible influence of internal tides on nutrient status and physiology. *Limnol. Oceanogr.,* **49,** 1923–1936.

Soloviev, A. V., M. E. Luther, and R. H. Weisberg, 2003: Energetic baroclinic super-tidal oscillations on the southeast Florida shelf. *Geophys. Res. Lett.,* **30,** 1463–1467.

Stommel, H., 1965: *The Gulf Stream—A Physical and Dynamical Description.* University of California Press, 248 pp.

Taylor, J. R., 1992: The energetics of breaking events in a resonantly forced internal wave field. *J. Fluid Mech.,* **239,** 309–340.

Thorpe, S. A., 2001a: Internal wave reflection and scatter from sloping rough topography. *J. Phys. Oceanogr.,* **31,** 537–553.

——, 2001b: On the reflection of internal wave groups from sloping topography. *J. Phys. Oceanogr.,* **31,** 3121–3126.

Wallace, B. C., and D. L. Wilkinson, 1988: Run-up of internal waves on a gentle slope in a 2-layered system. *J. Fluid Mech.,* **191,** 419–442.

Wolanski, E., and G. L. Pickard, 1983: Upwelling by internal tides and Kelvin waves at the continental shelf break on the Great Barrier Reef. *Aust. J. Mar. Res.,* **34,** 65–80.

——, and W. H. Hamner, 1988: Topographically controlled fronts in the ocean and their biological influence. *Science,* **241,** 177–181.

——, and B. Delesalle, 1995: Upwelling by internal waves, Tahiti, French Polynesia. *Cont. Shelf Res.,* **15,** 357–368.

——, and E. Deleersnijder, 1998: Island-generated internal waves at Scott Reef, Western Australia. *Cont. Shelf Res.,* **18,** 1649–1666.